2 ATLAS+CMS DARK MATTER FORUM RECOMMENDA-
3 TIONS

4 Author/contributor list to be added as document is finalized.
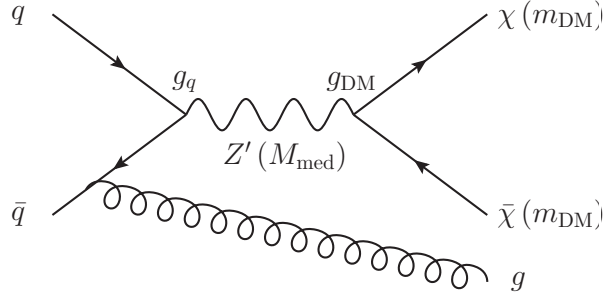
5 May 6, 2015

Figure 1.1: The diagram shows the pair production of dark matter particles in association with a parton from the initial state via an s-channel vector or axial-vector mediator. The process if specified by $(M_{\mathrm{med}}, m_{\mathrm{DM}}, g_{\mathrm{DM}}, g_q)$, the mediator and dark matter masses, and the mediator couplings to dark matter and quarks respectively.

1

Recommended models for all MET+X analyses

1.1 Vector and axial vector mediator, s-channel exchange

There are several matrix element implementations of the s-channel vector mediated DM production. This is available in POWHEG, MADGRAPH and also MCFM. The implementation in POWHEG generates DM pair production with 1 parton at next-to-leading order (NLO), whilst MADGRAPH and MCFM are at leading order (LO). As shown in POWHEG Ref. [HKR13], including NLO corrections result in an enhancement in the cross section as compared to LO and though this is not significant, it does lead to a substantial reduction in the dependence on the choice of the renormalization and factorization scale and hence the theoretical uncertainty on the signal prediction. Since NLO calculations are available for the process in POWHEG, we recommend to proceed with POWHEG as the generator of choice.

We consider the case of a dark matter particle that is a Dirac fermion and where the production proceeds via the exchange of a spin-1 s-channel mediator. We consider the following interactions between the DM and SM fields including a vector mediator with:

(a) vector couplings to DM and SM,

(b) axial-vector couplings to DM and SM.

The corresponding Lagrangians are

$$\mathcal{L}_{\text{vector}} = \sum_q g_q Z'_\mu \bar{q} \gamma^\mu q + g_{\text{DM}} Z'_\mu \bar{\chi} \gamma^\mu \chi \qquad (1.1)$$

$$\mathcal{L}_{\text{axial-vector}} = \sum_q g_q Z'_\mu \bar{q} \gamma^\mu \gamma^5 q + g_{\text{DM}} Z'_\mu \bar{\chi} \gamma^\mu \gamma^5 \chi \qquad (1.2)$$

where the coupling extends over all the quarks and universal cou-
plings are assumed for all the quarks. It is also possible to consider
another model in which mixed vector and axial-vector couplings
are considered, for instance the couplings to the quarks are vector
whereas those to DM are axial-vector. As a starting point, we con-
sider only the models with the vector couplings only and axial vector
couplings only.

We assume that no additional visible or invisible decays contribute
to the width of the mediator, this is referred to as the minimal width
and it is defined as follows for the vector and axial-vector models.

$$\Gamma_{\text{min}} = \Gamma_{\bar{\chi}\chi} + \sum_q \Gamma_{\bar{q}q} \qquad (1.3)$$

where the individual contributions to this from the partial width are
from

$$\Gamma^{\text{V}}_{\bar{\chi}\chi} = \frac{g_{\text{DM}}^2 M_{\text{med}}}{12\pi} \left(1 + \frac{2m_{\text{DM}}^2}{M_{\text{med}}^2}\right) \sqrt{1 - \frac{4m_{\text{DM}}^2}{M_{\text{med}}^2}} \qquad (1.4)$$

$$\Gamma^{\text{V}}_{\bar{q}q} = \frac{3g_q^2 M_{\text{med}}}{12\pi} \left(1 + \frac{2m_q^2}{M_{\text{med}}^2}\right) \sqrt{1 - \frac{4m_q^2}{M_{\text{med}}^2}} \qquad (1.5)$$

$$\Gamma^{\text{A}}_{\bar{\chi}\chi} = \frac{g_{\text{DM}}^2 M_{\text{med}}}{12\pi} \left(1 - \frac{4m_{\text{DM}}^2}{M_{\text{med}}^2}\right)^{3/2} \qquad (1.6)$$

$$\Gamma^{\text{A}}_{\bar{q}q} = \frac{3g_q^2 M_{\text{med}}}{12\pi} \left(1 - \frac{4m_q^2}{M_{\text{med}}^2}\right)^{3/2}. \qquad (1.7)$$

Note the color factor 3 in the quark terms. Figure 1.2 shows the min-
imal width as a function of mediator mass for both vector and axial-
vector mediators assuming couplings of 1. With this choice of the
couplings, the dominant contribution to the minimal width comes
from the quarks due to the color factor enhancement.

The simplified models described here have four free parameters:
mediator mass M_{med}, Dark Matter mass m_{DM}, coupling of the medi-
ator to quarks g_q and coupling of the mediator to Dark Matter g_{DM}.
In order to determine an optimal choice of the parameter grid for
presentation of the early Run-2 results, dependencies of the kinematic
quantities and cross sections on the individual parameters need to be
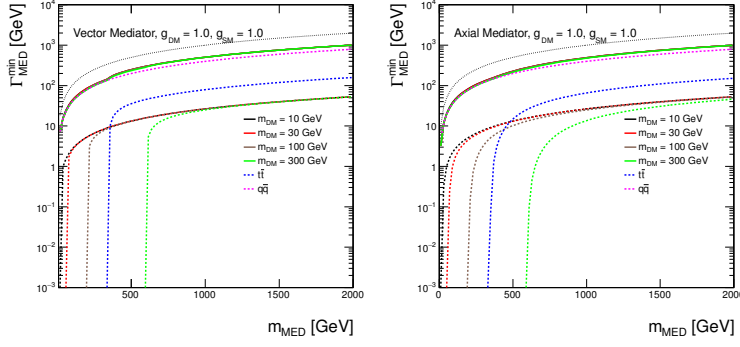studied. The following paragraphs list the main observations from

Figure 1.2: Minimal width as a function of mediator mass for vector and axial-vector mediator assuming couplings of 1. The total width is shown as solid lines for Dark Matter masses of 10 GeV, 30 GeV, 100 GeV and 300 GeV in black, red, brown and green, respectively. The individual contributions from Dark Matter are indicated by dotted lines with the same colors. The contribution from all quarks but top is shown as magenta dotted line and the contribution from top quarks only is illustrated by the dotted blue line. The dotted black line shows the extreme case $\Gamma_{min} = M_{med}$.

the scans over the parameters that support the final proposal for the parameter grid.

Scan over the couplings Figure 1.3 reveals there are no differences in the shape of the $\not{E}_T$ distribution among the samples where the pair of 10 GeV Dark Matter particles are produced on-shell from the mediator of 1 TeV, generated with different choice of the coupling strength. The considered coupling values range from 0.1 to 1.45, where the latter value approximates the maximum allowed coupling value, holding $g_q = g_{DM}$, such that $\Gamma_{min} < M_{med}$. Based on similar plots for different choices of mediator and Dark Matter masses, it is concluded that the shapes of kinematic distributions are not altered neither for the on-shell Dark Matter production where $M_{med} > 2m_{DM}$, nor for the off-shell Dark Matter production where $M_{med} < 2m_{DM}$. Only the cross sections change. Differences in kinematic distributions are expected only close to the transition region where both on-shell and off-shell regimes mix.
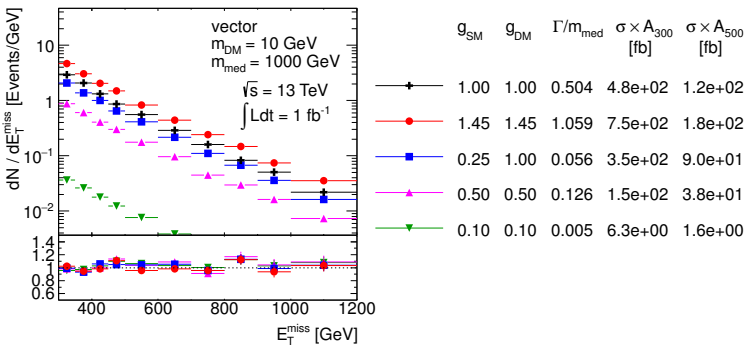

Figure 1.3: Scan over couplings. The $\not{E}_T$ distribution is compared for the vector mediator models using the parameters as indicated. Ratios of the normalized distributions with respect to the first one are shown. A_{300} and A_{500} in the table denote the acceptance of the $\not{E}_T > 300$ GeV and $\not{E}_T > 500$ GeV cut, respectively.

The only place where special care needs to be taken are extremely heavy and narrow mediators, in other words with low couplings. Figure 1.4 suggests a change in the shape of the $\not{E}_T$ distribution for 5 TeV mediator once Γ_{min}/M_{med} gets down to the order of percent or

72 below. This, however, does not come from physics as it is a feature of
73 the generator implementation, where a cutoff for the regions far away
74 from the mediator mass is often used. This is illustrated in Fig. 1.5
75 showing the invariant mass of the Dark Matter pair in the samples
76 generated for 7 TeV mediator with different coupling strength. In
77 all cases, it is expected to observe a peak around the mediator mass
78 with a tail extending to $m_{\bar{\chi}\chi} \to 0$, significantly enhanced by parton
79 distribution functions at low Bjorken x. For coupling strength 1 and
80 3, the massive enhancement at $m_{\bar{\chi}\chi} \to 0$ implies the resonant pro-
81 duction at $m_{\bar{\chi}\chi} = 7$ TeV is statistically suppressed such that barely
82 any events are generated there. However, for narrower mediators
83 with couplings below 1, the peak around 7 TeV is clearly visible in
84 the generated sample and the dominant tail at $m_{\bar{\chi}\chi} \to 0$ is artificially
85 cut off, leading to unphysical cross section predictions and kinematic
86 shapes. This explains why the sample with the narrowest mediator in
87 Fig. 1.4 is heavily suppressed in terms of production cross section and
88 also gives different $\not{E}_T$ shape. In general, for such extreme parameter
89 choices the EFT model should give the correct answer. In case the
90 simplified model calculation does not reproduce the EFT result, the
91 phase space generation of the simplified model has to be carefully ex-
92 amined in order to understand the cause of the problem. Fortunately,
93 this is a rather academic discussion as such extreme corners of the
94 parameter space are not going to be considered for presentation of
95 Run-2 results.

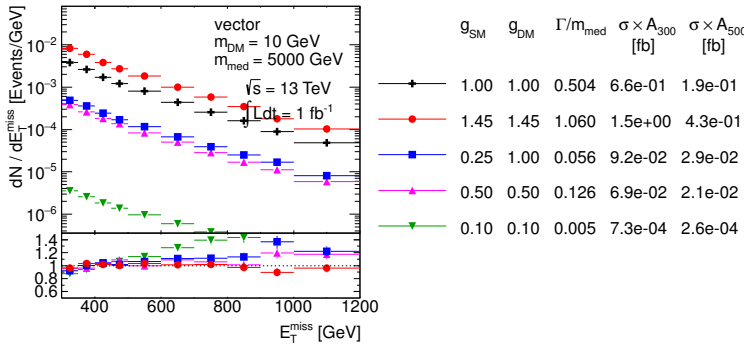| g_{SM}	g_{DM}	Γ/m_{med}	$\sigma \times A_{300}$ [fb]	$\sigma \times A_{500}$ [fb]
1.00	1.00	0.504	6.6e-01	1.9e-01
1.45	1.45	1.060	1.5e+00	4.3e-01
0.25	1.00	0.056	9.2e-02	2.9e-02
0.50	0.50	0.126	6.9e-02	2.1e-02
0.10	0.10	0.005	7.3e-04	2.6e-04

Figure 1.4: Scan over couplings. The $\not{E}_T$ distribution is compared for the vector mediator models using the parameters as indicated. Ratios of the normalized distributions with respect to the first one are shown. A_{300} and A_{500} in the table denote the acceptance of the $\not{E}_T > 300$ GeV and $\not{E}_T > 500$ GeV cut, respectively.

96   *Scan over the Dark Matter mass*   For the fixed mediator mass and cou-
97   plings, both the cross section and the kinematic distributions remain
98   similar for different Dark Matter masses as long as $M_{\mathrm{med}} > 2m_{\mathrm{DM}}$.
99   This is illustrated in Fig. 1.6 on an example of 1 TeV mediator and
100 Dark Matter mases ranging from 10 GeV to 300 GeV. It is observed
101 that the cross section decreases as the Dark Matter mass reaches
102 closer to $M_{\mathrm{med}}/2$. Once the Dark Matter pair is produced off-line,
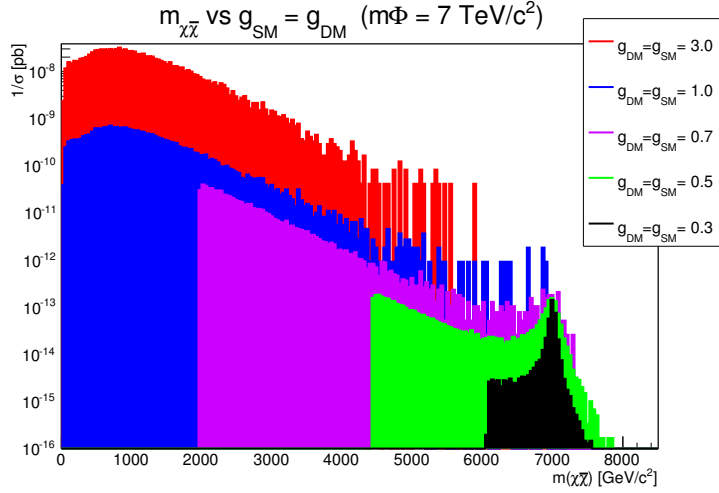103 the cross section of such simplified model is suppressed and the $\not{E}_T$

Figure 1.5: Invariant mass of the Dark Matter pair in the samples with $M_{\mathrm{med}} = 7\,\mathrm{TeV}$ and different coupling strengths.

spectrum hardens, as demonstrated with the choice of 1 TeV Dark Matter in the same plot. Figure 1.7 reveals the $\not{E}_T$ spectrum hardens further with increasing Dark Matter mass, accompanied by the gradual decrease of the cross section. From these observations one can conclude:

- A coarse binning along m_{DM} is sufficient at $M_{\mathrm{med}} \gg 2m_{\mathrm{DM}}$.

- Finer binning is needed in order to capture the changes in the cross section and kinematic quantities close to the production threshold on both sides around $M_{\mathrm{med}} = 2m_{\mathrm{DM}}$.

- Due to the significant cross section suppression of the off-shell Dark Matter pair production, it is not necessary to populate the parameter space $M_{\mathrm{med}} \ll 2m_{\mathrm{DM}}$ since the LHC is not going to be able to probe the models there.

Figure 1.6: Scan over Dark Matter mass. The $\not{E}_T$ distribution is compared for the vector mediator models using the parameters as indicated. Ratios of the normalized distributions with respect to the first one are shown. A_{300} and A_{500} in the table denote the acceptance of the $\not{E}_T > 300\,\mathrm{GeV}$ and $\not{E}_T > 500\,\mathrm{GeV}$ cut, respectively.

Scan over the mediator mass Changing the mediator mass for fixed Dark Matter mass and couplings leads to significant differences in
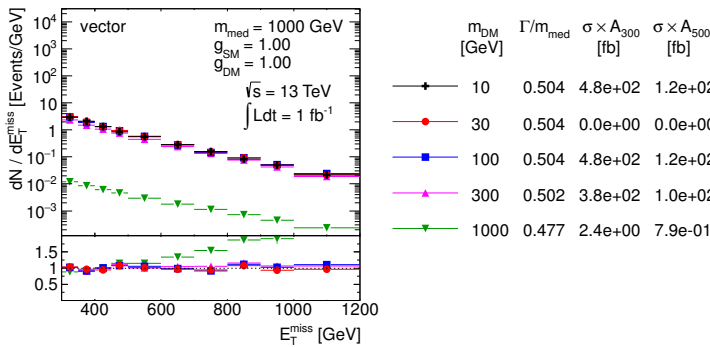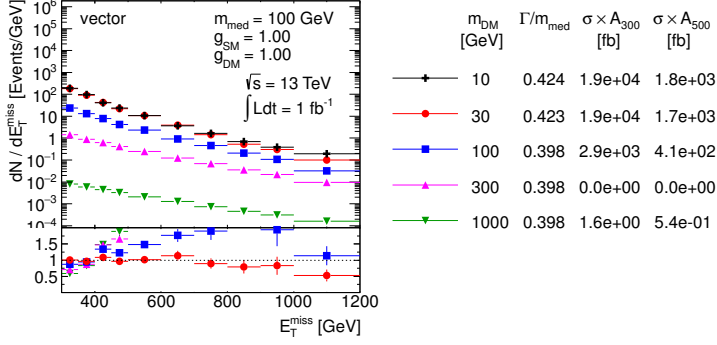
Figure 1.7: Scan over Dark Matter mass. The $\not{E}_T$ distribution is compared for the vector mediator models using the parameters as indicated. Ratios of the normalized distributions with respect to the first one are shown. A_{300} and A_{500} in the table denote the acceptance of the $\not{E}_T > 300\,\text{GeV}$ and $\not{E}_T > 500\,\text{GeV}$ cut, respectively.

119 cross section and shapes of the kinematic variables for $M_{\text{med}} > 2m_{\text{DM}}$
120 as shown in Fig. 1.8. As expected, higher mediator masses lead to
121 harder $\not{E}_T$ spectra. On the other hand, the $\not{E}_T$ shapes are similar
122 in the off-shell Dark Matter production regime as well as no dra-
123 matic differences in cross sections are observed, which is illustrated
124 in Fig. 1.9. Therefore, a coarse binning along m_{DM} is sufficient at
125 $M_{\text{med}} \ll 2m_{\text{DM}}$.

Figure 1.8: Scan over mediator mass. The $\not{E}_T$ distribution is compared for the vector mediator models using the parameters as indicated. Ratios of the normalized distributions with respect to the first one are shown. A_{300} and A_{500} in the table denote the acceptance of the $\not{E}_T > 300\,\text{GeV}$ and $\not{E}_T > 500\,\text{GeV}$ cut, respectively.
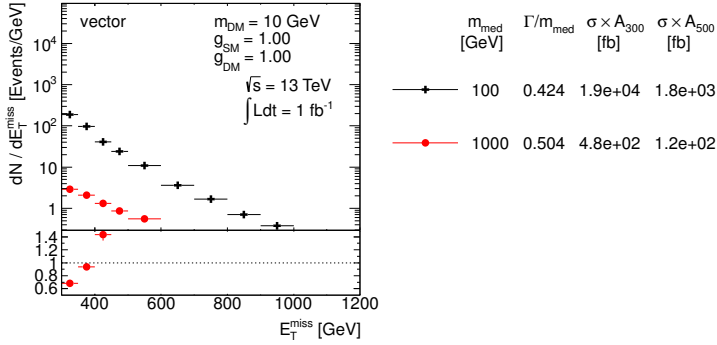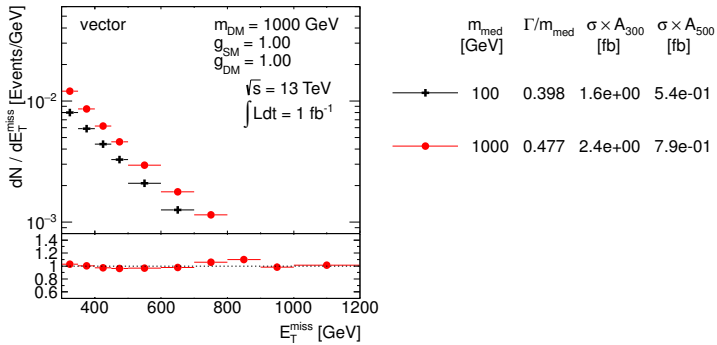

Figure 1.9: Scan over mediator mass. The $\not{E}_T$ distribution is compared for the vector mediator models using the parameters as indicated. Ratios of the normalized distributions with respect to the first one are shown. A_{300} and A_{500} in the table denote the acceptance of the $\not{E}_T > 300\,\text{GeV}$ and $\not{E}_T > 500\,\text{GeV}$ cut, respectively.

126 *Proposed parameter grid*   Based on the observations above, the follow-
127 ing proposal is made for the presentation of the early Run-2 results

from the LHC:

(a) Give results in the M_{med}–m_{DM} plane for a particular choice of the couplings.

(b) Give results in the g_q–g_{DM} plane for a particular choice of the masses.

We choose to display the results in the M_{med}–m_{DM} plane for the choice of the couplings $g_q = g_{\mathrm{DM}} = 1$. In order to motivate the highest mediator mass grid point, the expected sensitivity of Run-2 LHC data needs to be taken into account. The expected upper limit at 95% confidence level on the product of cross section, acceptance and efficiency, $\sigma \times A \times \epsilon$, in the final Run-1 ATLAS mono-jet anaylsis [A$^+$15] is 51 fb and 7.2 fb for $\not{E}_T > 300$ GeV and $\not{E}_T > 500$ GeV, respectively. The ATLAS 14 TeV prospects [ATL14] predict twice better sensitivity with the first 5 fb^{-1} of data already. Given the cross section for V+jets processes increases by roughly factor 2 when going from $\sqrt{s} = 8$ TeV to 13 TeV, similar fiducial cross section limits can be expected with the first Run-2 data as from the final Run-1 analysis. The generator level cross section times the acceptance at $\not{E}_T > 500$ GeV for the model with couplings $g_q = g_{\mathrm{DM}} = 1$, light Dark Matter of 10 GeV and 1 TeV vector mediator is at the order of 100 fb, i.e. the early Run-2 mono-jet analysis is going to be sensitive to heavier mediators than this. The value of $\sigma \times A$ at $\not{E}_T > 500$ GeV for 5 TeV vector mediator is at the order of 0.1 fb, therefore this model probably lies beyond the reach of the LHC. Based on these arguments, the following M_{med} grid points are chosen, equidistant in the logarithmic scale: 10 GeV, 30 GeV, 100 GeV, 300 GeV, 1000 GeV and 3000 GeV. Given the fact that significant changes in cross section happen around the $M_{\mathrm{med}} = 2m_{\mathrm{DM}}$ threshold, the m_{DM} grid points are taken at $M_{\mathrm{med}}/2$, namely: 5 GeV, 15 GeV, 50 GeV, 150 GeV, 500 GeV and 1500 GeV. The detailed studies of the impact of the parameter changes on the cross section and kinematic distributions presented earlier in this section support removing some of the grid points and rely on interpolation. The optimised grids proposed for the vector and axial-vector mediators are given in Fig. 1.10, containing 24 mass points each.

The presentation of the results in the g_q–g_{DM} plane for fixed masses benefits from cross section scaling and is discussed in Section 1.3.

1.2 Scalar and pseudoscalar mediator, s-channel exchange

The matrix element implementation of the s-channel spin-0 mediated DM production is available in POWHEG with the full top-loop calculation at LO [HR15]. The model assumes Dirac Dark Matter particles and is based on the minimal flavor violation (MFV), which motivates
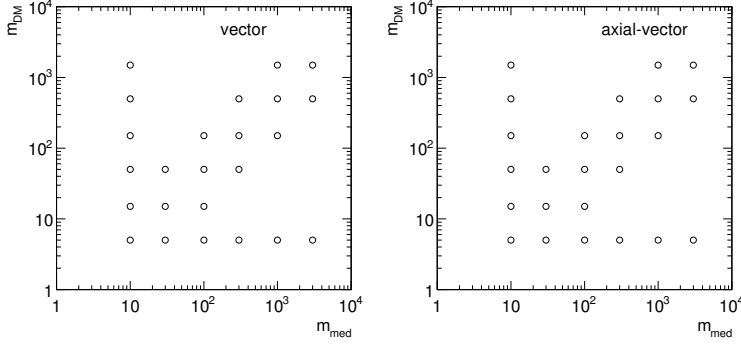
Figure 1.10: Proposed parameter grid for vector and axial-vector mediator in the M_{med}–m_{DM} plane.

Higgs-like Yukawa couplings of the mediator to the Standard Model quarks. No other couplings, such as to leptons, are allowed in this model. The following two cases are considered:

(a) scalar couplings to DM and SM,

(b) pseudo-scalar couplings to DM and SM

with the corresponding Lagrangians written as:

$$\mathcal{L}_{\text{scalar}} = g_q \sum \frac{m_q}{v}(\bar{q}q)S + g_{\text{DM}}(\bar{\chi}\chi)S \tag{1.8}$$

$$\mathcal{L}_{\text{pseudo-scalar}} = g_q \sum \frac{m_q}{v}(\bar{q}\gamma^5 q)P + g_{\text{DM}}(\bar{\chi}\gamma^5\chi)P \tag{1.9}$$

$$\tag{1.10}$$

where $v = 246\,\text{GeV}$ denotes the Higgs vacuum expectation value.

We choose to consider minimal mediator width given by Eq. 1.3, where the individual contributions follow from

$$\Gamma_{\bar{\chi}\chi}^{S} = \frac{g_{\text{DM}}^2 M_{\text{med}}}{8\pi}\left(1 - \frac{4m_{\text{DM}}^2}{M_{\text{med}}^2}\right)^{3/2} \tag{1.11}$$

$$\Gamma_{\bar{q}q}^{S} = \frac{3g_q^2 M_{\text{med}}}{8\pi}\frac{m_q^2}{v^2}\left(1 - \frac{4m_q^2}{M_{\text{med}}^2}\right)^{3/2} \tag{1.12}$$

$$\Gamma_{\bar{\chi}\chi}^{P} = \frac{g_{\text{DM}}^2 M_{\text{med}}}{8\pi}\sqrt{1 - \frac{4m_{\text{DM}}^2}{M_{\text{med}}^2}} \tag{1.13}$$

$$\Gamma_{\bar{q}q}^{P} = \frac{3g_q^2 M_{\text{med}}}{8\pi}\frac{m_q^2}{v^2}\sqrt{1 - \frac{4m_q^2}{M_{\text{med}}^2}}\ . \tag{1.14}$$

The minimal width for scalar and pseudo-scalar mediators with $g_q = g_{\text{DM}} = 1$ are shown in Fig. 1.11, illustrating the effect of the Higgs-like Yukawa couplings. For the mediator masses above twice the top quark mass m_t, the minimal width receives the dominant contribution from the top quark. For lighter mediator masses, Dark Matter dominates as the couplings to lighter quarks are Yukawa suppressed. Note that we decide to ignore the partial width coming from gluons through loops as it can be safely neglected [HR15].
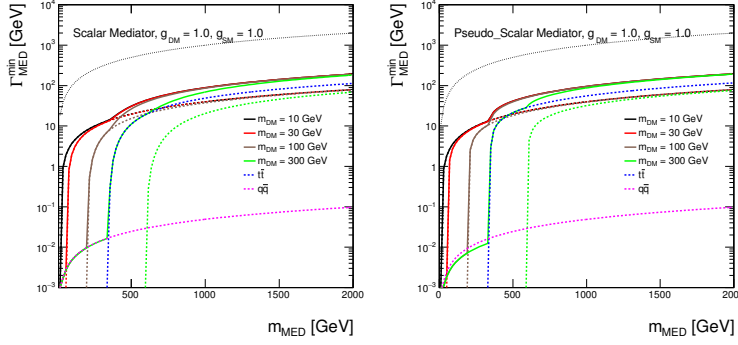
Figure 1.11: Minimal width as a function of mediator mass for scalar and pseudo-scalar mediator assuming couplings of 1. The total width is shown as solid lines for Dark Matter masses of 10 GeV, 30 GeV, 100 GeV and 300 GeV in black, red, brown and green, respectively. The individual contributions from Dark Matter are indicated by dotted lines with the same colors. The contribution from all quarks but top is shown as magenta dotted line and the contribution from top quarks only is illustrated by the dotted blue line. The dotted black line shows the extreme case $\Gamma_{\min} = M_{\mathrm{med}}$.

Similarly as in the case of the vector and axial-vector mediators, scans in the paramater space are performed also for the scalar and pseudo-scalar mediators in order to decide on the optimised parameter grid for the presentation of Run-2 results. Figures **??** show the scans over the couplings, Dark Matter mass and mediator mass and the same conclusions apply as in Section 1.1.

Since the top quark gives the dominant contribution to the mediator width due to Higgs-like Yukawa couplings, the effect of the top channel opening in the mediator production was studied in addition. Scan over the mediator mass is shown in Fig. 1.16 where the mediator masses 300 GeV and 500 GeV are chosen to be below and above $2m_t$. The off-shell Dark Matter production regime is assumed by taking $m_{\mathrm{DM}} = 1$ TeV in order to allow studying solely the effects of the couplings to quarks. No differences in the kinematic distributions are observed and also the cross sections remain similar in this case. Therefore, it is concluded that no significant changes appear for mediator masses around the $2m_t$ threshold.

Figure 1.12: Scan over couplings. The $\not{E}_T$ distribution is compared for the scalar mediator models using the parameters as indicated. Ratios of the normalized distributions with respect to the first one are shown. A_{300} and A_{500} in the table denote the acceptance of the $\not{E}_T > 300$ GeV and $\not{E}_T > 500$ GeV cut, respectively.

The optimized parameter grid in the M_{med}–m_{DM} plane for scalar and pseudo-scalar mediators is motivated by similar arguments as in the previous section. Therefore, similar pattern is followed here, taking again $g_q = g_{\mathrm{DM}} = 1$. Only the sensitivity to the highest me-

m_{DM} [GeV]	Γ/m_{med}	$\sigma \times A_{300}$ [fb]	$\sigma \times A_{500}$ [fb]
10	0.062	3.3e+01	4.0e+00
30	0.061	3.1e+01	4.1e+00
100	0.053	2.5e+01	3.2e+00
300	0.022	1.3e-01	2.6e-02
1000	0.022	3.4e-05	1.2e-05

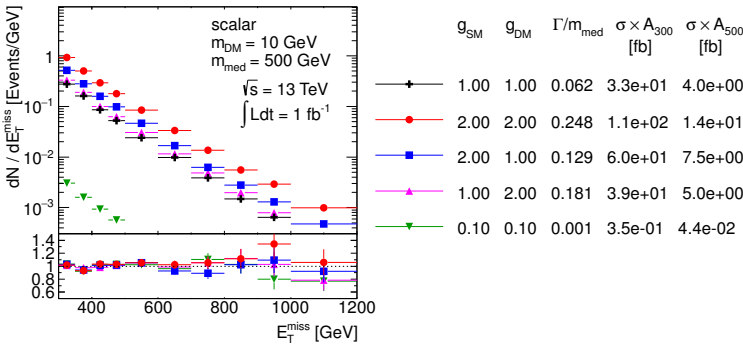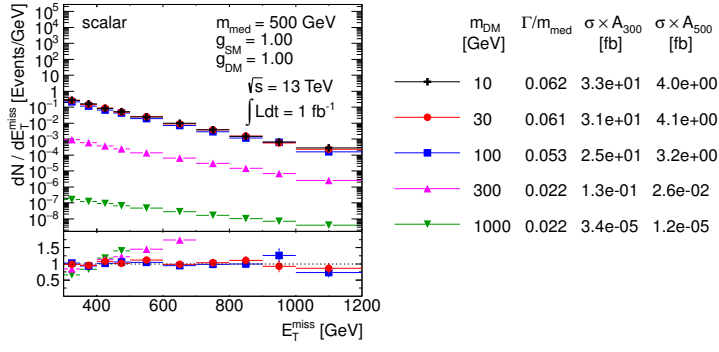Figure 1.13: Scan over Dark Matter mass. The $\not{E}_T$ distribution is compared for the scalar mediator models using the parameters as indicated. Ratios of the normalized distributions with respect to the first one are shown. A_{300} and A_{500} in the table denote the acceptance of the $\not{E}_T > 300\,\mathrm{GeV}$ and $\not{E}_T > 500\,\mathrm{GeV}$ cut, respectively.

m_{DM} [GeV]	Γ/m_{med}	$\sigma \times A_{300}$ [fb]	$\sigma \times A_{500}$ [fb]
10	0.037	8.0e+01	7.0e+00
30	0.020	4.5e+01	3.8e+00
100	0.000	1.2e+00	1.5e-01
300	0.000	5.3e-02	1.1e-02
1000	0.000	3.2e-05	1.1e-05

Figure 1.14: Scan over Dark Matter mass. The $\not{E}_T$ distribution is compared for the scalar mediator models using the parameters as indicated. Ratios of the normalized distributions with respect to the first one are shown. A_{300} and A_{500} in the table denote the acceptance of the $\not{E}_T > 300\,\mathrm{GeV}$ and $\not{E}_T > 500\,\mathrm{GeV}$ cut, respectively.

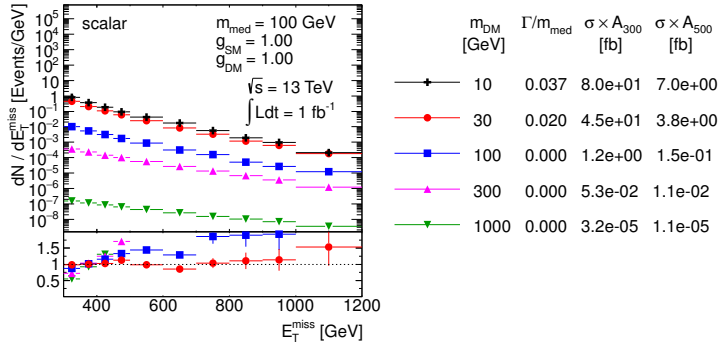| m_{med} [GeV]	Γ/m_{med}	$\sigma \times A_{300}$ [fb]	$\sigma \times A_{500}$ [fb]
100	0.037	8.0e+01	7.0e+00
300	0.040	6.2e+01	6.5e+00
500	0.062	3.3e+01	4.0e+00

Figure 1.15: Scan over mediator mass. The $\not{E}_T$ distribution is compared for the scalar mediator models using the parameters as indicated. Ratios of the normalized distributions with respect to the first one are shown. A_{300} and A_{500} in the table denote the acceptance of the $\not{E}_T > 300\,\mathrm{GeV}$ and $\not{E}_T > 500\,\mathrm{GeV}$ cut, respectively.

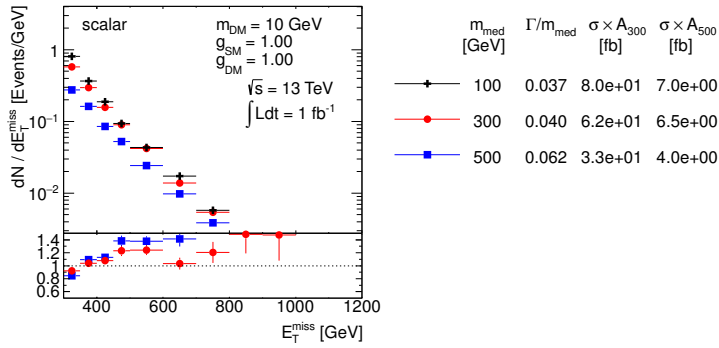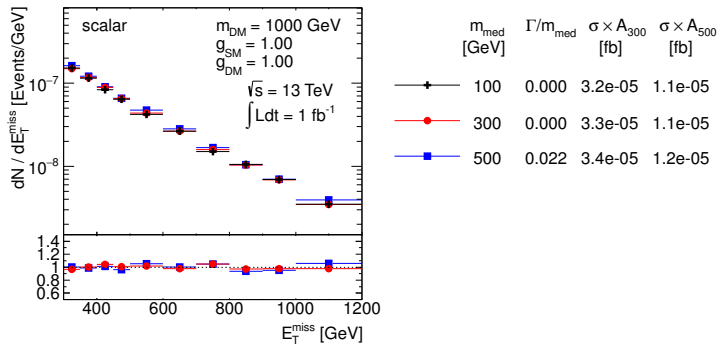| m_{med} [GeV]	Γ/m_{med}	$\sigma \times A_{300}$ [fb]	$\sigma \times A_{500}$ [fb]
100	0.000	3.2e-05	1.1e-05
300	0.000	3.3e-05	1.1e-05
500	0.022	3.4e-05	1.2e-05

Figure 1.16: Scan over mediator mass. The $\not{E}_T$ distribution is compared for the scalar mediator models using the parameters as indicated. Ratios of the normalized distributions with respect to the first one are shown. A_{300} and A_{500} in the table denote the acceptance of the $\not{E}_T > 300\,\mathrm{GeV}$ and $\not{E}_T > 500\,\mathrm{GeV}$ cut, respectively.

205 diator masses has to be revisited. The generator level cross section
206 times the acceptance at $\not{E}_T > 500\,\text{GeV}$ for the model with couplings
207 $g_q = g_{\text{DM}} = 1$, light Dark Matter of 10 GeV and 500 GeV scalar me-
208 diator is at the order of 10 fb, i.e. just at the edge of the early Run-2
209 sensitivity. Increasing the mediator mass to 1 TeV pushes the prod-
210 uct $\sigma \times A$ down to approximately 0.1 fb, beyond the LHC sensitivity.
211 Therefore, we choose to remove the 3 TeV mediator mass from the
212 grid and present the final grid with 19 mass points only in Fig. 1.17.
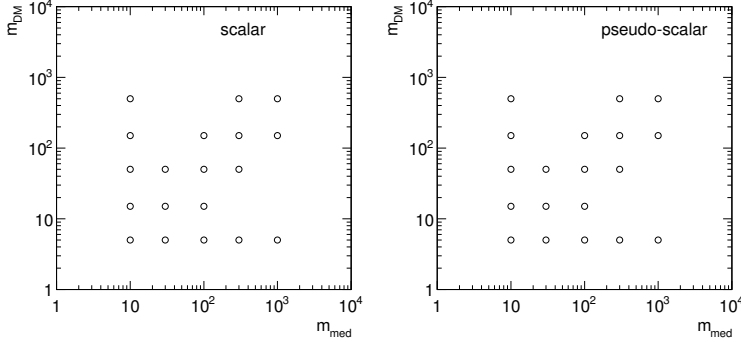

Figure 1.17: Proposed parameter grid for scalar and pseudo-scalar mediator in the M_{med}–m_{DM} plane.

213   The proposal for the scan in the g_q–g_{DM} plane is described in the
214 following section.

1.3   *Cross section scaling*

216 The aim of the parameter grid optimization is to find out whether
217 certain parts of the parameter space can be omitted and one can rely
218 on the neighboring grid points in order to populate the missing parts.
219 There are two ways of doing this:

220 • Interpolation is used in-between the grid points that are close
221   enough such that finer granularity is not needed for the presenta-
222   tion purposes, or between the points where smooth or no changes
223   of the results are expected. The latter argument is exactly the one
224   that motivates the reduction of the grid points in the M_{med}–m_{DM}
225   plane.

226 • Recalculation of the results can be used when the dependencies
227   with respect to the neighboring grid points are known.

228   The results of the scan over the couplings presented in the previ-
229 ous sections indicate there are no changes in kinematic distributions
230 for different choices of the coupling strengths. This means that the
231 acceptance remains the same in the whole g_q–g_{DM} plane and it is
232 sufficient to perform the detector simulation only for one single grid
233 point. The resulting truth-level selection acceptance and the detector

reconstruction efficiency can then be applied to all remaining grid points in the g_q–g_{DM} plane where only the generator-level cross section needs to be known. This significantly reduces the computing time as the detector response is by far the most expensive part of the Monte Carlo sample production. However, a further step can be taken if a parameterization of the cross section dependence from one grid point to another exists, in which case the number of generated samples can be reduced even further.

Let us now elaborate on a cross section scaling procedure. The propagator on the s-channel exchange is written in a Breit-Wigner form as $\frac{1}{\sqrt{s}-M_{\mathrm{med}}^2+iM_{\mathrm{med}}\Gamma}$. The relative size of the center-of-mass energy defined by the two partons entering the hard process and the mediator mass allows to classify the production in the following way:

- off-shell production when $\sqrt{s} \gg M_{\mathrm{med}}$ leading to suppressed cross sections,

- on-shell production when $\sqrt{s} \sim M_{\mathrm{med}}$ leading to enhanced cross sections,

- effective field theory (EFT) limit when $\sqrt{s} \ll M_{\mathrm{med}}$.

All three categories can be distinguished in Fig. 1.18 showing the upper limit on the interaction scale $M^* \equiv M_{\mathrm{med}}/\sqrt{g_q g_{DM}}$ for vector mediator. In the case of the off-shell production and the EFT limit, the first term in the propagator dominates which reduces the dependence on the mediator width. Therefore, in these cases one can approximate the cross section as

$$\sigma \propto g_q^2 g_{DM}^2. \tag{1.15}$$

The on-shell production regime is the most interesting one as it gives the best chances for a discovery at the LHC given the cross section enhancement. The propagator term with the width cannot be neglected in this case and, in the narrow width approximation, one can integrate

$$\int \frac{ds}{(s-M_{\mathrm{med}}^2)^2 + M_{\mathrm{med}}^2\Gamma^2} = \frac{\pi}{M_{\mathrm{med}}\Gamma} \tag{1.16}$$

which further implies the cross section scaling

$$\sigma \propto \frac{g_q^2 g_{DM}^2}{\Gamma}. \tag{1.17}$$

Since $\Gamma \sim g_q^2 + g_{DM}^2$, one can simplify this rule in the extreme cases as follows

$$\sigma \quad \propto \quad \frac{g_q^2 g_{DM}^2}{g_q^2 + g_{DM}^2} \xrightarrow{g_q \ll g_{DM}} g_q^2 \tag{1.18}$$

$$\sigma \quad \propto \quad \frac{g_q^2 g_{DM}^2}{g_q^2 + g_{DM}^2} \xrightarrow{g_q \gg g_{DM}} g_{DM}^2. \tag{1.19}$$

254 However, it is important to keep in mind that there is no simple
255 scaling rule for how the cross section changes with the Dark Matter
256 mass, mediator mass and the mediator width because PDFs matter in
257 such cases as well. Therefore, the scaling procedure outlined above is
258 expected to work only for fixed masses and fixed mediator width.
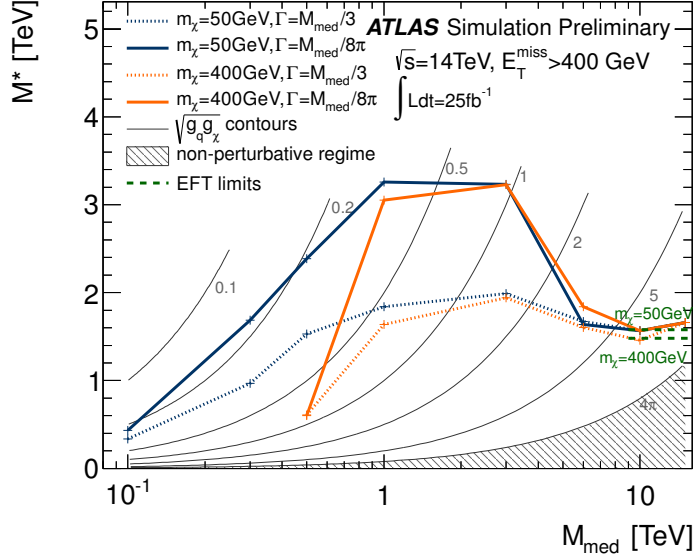

Figure 1.18: Comparison of the 95%
CL lower limits on the scale of the
interaction of a Z'-like simplified model
at 14 TeV, in terms of the mediator
mass. Corresponding limits from
EFT models are shown on the same
plot as green dashed lines to show
equivalence between the two models
for high mediator masses. Taken from
Ref. [ATL14].

259 Figures 1.19 and 1.20 show the minimal width in the g_q–g_{DM} plane
260 for all vector, axial-vector, scalar and pseudo-scalar mediators for
261 $M_{med} = 100\,\text{GeV}$ and 1000 GeV, respectively, taking $m_{DM} = 10\,\text{GeV}$.
262 The individual colors indicate the lines of constant width along
263 which the cross section scaling works. For vector and axial-vector
264 mediators, the minimal width is predominantly defined by g_q due
265 to the number of quark flavors and the color factor. On the contrary,
266 both the Standard Model and Dark Matter partial width have com-
267 parable contributions in case of scalar and pseudo-scalar mediators
268 if the top quark channel is open ($M_{med} > 2m_t$). However, mostly
269 g_{DM} defines the minimal width for $M_{med} < 2m_t$ due to the Yukawa-
270 suppressed light quark couplings.
271 The performance of the cross section scaling is demonstrated in
272 Fig. 1.21 where the mass point $M_{med} = 1\,\text{TeV}$ and $m_{DM} = 10\,\text{GeV}$ is
273 chosen and rescaled from the starting point $g_q = g_{DM} = 1$ accord-
274 ing to Eq. 1.17 to populate the whole g_q–g_{DM} plane. This means the
275 width is not kept constant in this test and this is done in purpose
276 in order to point out deviations from the scaling when the width is
277 altered. For each mass point, the rescaled cross section is compared
278 to the generator cross section and the ratio of the two is plotted.
279 For the given choice of the mass points, the scaling seems to work

Figure 1.19: Minimal width for vector, axial-vector, scalar and pseudo-scalar mediators as a function of the individual couplings g_q and g_{DM}, assuming $M_{med} = 100\,\mathrm{GeV}$ and $m_{DM} = 10\,\mathrm{GeV}$.
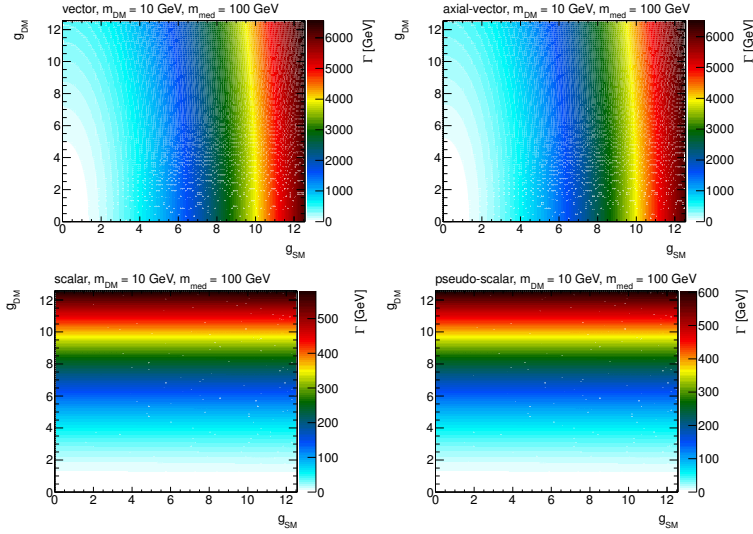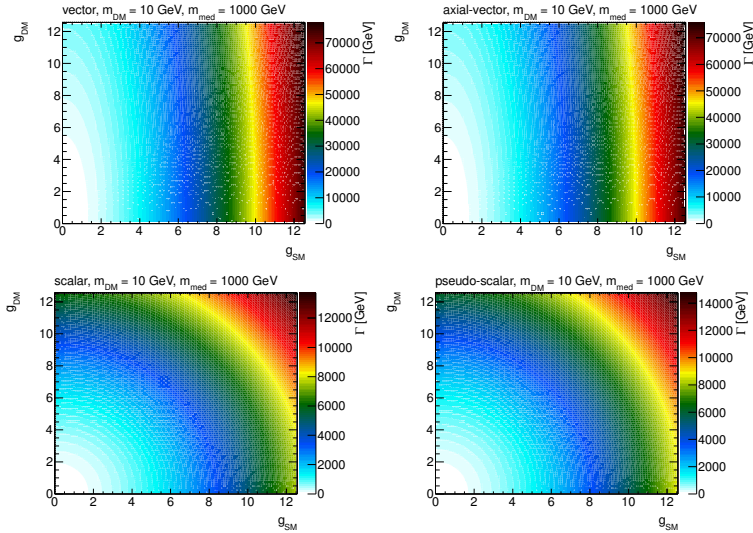
Figure 1.20: Minimal width for vector, axial-vector, scalar and pseudo-scalar mediators as a function of the individual couplings g_q and g_{DM}, assuming $M_{med} = 1\,\mathrm{TeV}$ and $m_{DM} = 10\,\mathrm{GeV}$.

approximately with the precision of $\sim 20\%$ in the region where $\Gamma_{\text{min}} < M_{\text{med}}$. Constant colors indicate the lines along which the cross section scaling works precisely and there is a remarkable resemblance of the patterns shown in the plots of the mediator width. To prove the scaling along the lines of constant width works, one such line is chosen in Fig. 1.22 for a scalar mediator, defined by $M_{\text{med}} = 300\,\text{GeV}$, $m_{\text{DM}} = 100\,\text{GeV}$, $g_q = g_{\text{DM}} = 1$, and the rescaled and generated cross sections are found to agree within 3%.
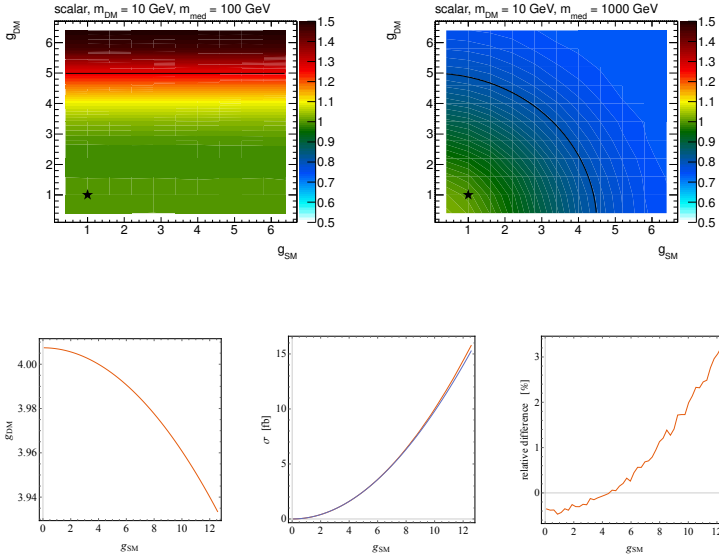

Figure 1.21: Ratio of the rescaled and generated cross sections in the g_q–g_{DM} plane. The point at $g_q = g_{\text{DM}} = 1$, taken as a reference for the rescaling, is denoted by a star symbol. Scalar model with $M_{\text{med}} = 100\,\text{GeV}$ (left) and 1 TeV (right) is plotted for $m_{\text{DM}} = 10\,\text{GeV}$. The limiting case $\Gamma_{\text{min}} = M_{\text{med}}$ is shown as a black line.

Figure 1.22: Scaling along the lines of constant width. The line of constant width for $M_{\text{med}} = 300\,\text{GeV}$ and $m_{\text{DM}} = 100\,\text{GeV}$, intercepting $g_q = g_{\text{DM}} = 4$ is shown on left. The generated and rescaled cross sections are compared in the middle, the corresponding ratio is shown on right.

Proposed parameter grid   We propose to present the results in the g_q–g_{DM} plane using the following prescription:

- Since the shapes of kinematic quantities do not change for different couplings, use the acceptance and efficiency for the available $m_{\text{DM}} = 50\,\text{GeV}$, $M_{\text{med}} = 300\,\text{GeV}$, $g_q = g_{\text{DM}} = 1$ grid point from the M_{med}–m_{DM} plane for the scalar and pseudo-scalar mediator. In case of the vector and axial-vector mediator, use the grid point $m_{\text{DM}} = 50\,\text{GeV}$, $M_{\text{med}} = 1\,\text{TeV}$, $g_q = g_{\text{DM}} = 1$.

- Generate additional samples in order to get generator cross sections only. For scalar and pseudo-scalar mediator, choose $m_{\text{DM}} = 50\,\text{GeV}$, $M_{\text{med}} = 300\,\text{GeV}$ with the following values for $g_q = g_{\text{DM}}$: 0.1, 2, 3, 4, 5, 6. For vector and axial vector mediator, choose $m_{\text{DM}} = 50\,\text{GeV}$, $M_{\text{med}} = 1\,\text{TeV}$ with the following values for $g_q = g_{\text{DM}}$: 0.1, 0.25, 0.5, 0.75, 1.25, 1.5. The upper values are defined by the minimal width reaching the mediator mass.

- Rescale the generator cross sections along the lines of constant width in order to populate the whole g_q–g_{DM} plane.

Rescaling to different mediator width   In general there may be an interest to consider larger mediator masses than Γ_{min} in order to accommodate further couplings of the mediator. The cross section scaling method described above can be used to reinterpret the results presented for the minimal width, since multiplying the width by factor n is equivalent to changing the coupling strength by factor $\sqrt{n}$, i.e.

$$\sigma(g_q, g_{DM}, n\Gamma_{min}(g_q, g_{DM})) \propto \frac{g_q^2 g_{DM}^2}{\Gamma_{min}(\sqrt{n}g_q, \sqrt{n}g_{DM})} \ . \qquad (1.20)$$

The cross section for the sample with couplings g_q and g_{DM} and modified mediator width $\Gamma = n\Gamma_{min}$ can therefore be rescaled from a sample generated with the minimal width corresponding to the couplings scaled by $\sqrt{n}$ as described in the following formula.

$$\sigma(g_q, g_{DM}, n\Gamma_{min}(g_q, g_{DM})) = \frac{1}{n^2}\sigma(\sqrt{n}g_q, \sqrt{n}g_{DM}, \Gamma_{min}(\sqrt{n}g_q, \sqrt{n}g_{DM}))$$
$$(1.21)$$

Advantage of doing this is again in the fact that no event selection and detector response needs to be simulated since the changes in couplings do not have an effect on the shapes of kinematic distributions.

1.3.1   *POWHEG settings*

This section describes specif settings for the Dark Matter models needed to run the POWHEG generation.

- The POWHEG implementation allows to generate a single sample that provides sufficient statistics in all mono-jet analysis signal regions. POWHEG generates weighted events and the `bornsuppfact` parameter is used to set the event suppression factor according to

$$F(k_T) = \frac{k_T^2}{k_T^2 + \texttt{bornsuppfact}^2} \ . \qquad (1.22)$$

  In this way, the events at low $\not{E}_T$ are suppressed and receive higher event weights which ensures higher statistics at high $\not{E}_T$. We recommend to set `bornsuppfact` to 1000.

- The `bornktmin` parameter allows to suppress the low $\not{E}_T$ region even further by starting the generation at a certain value of k_T. It is recommended to set this parameter to half the lower analysis $\not{E}_T$ cut, therefore the proposed value for `bornktmin` is 150.

- Set `runningwidth` to 0.

- Set `mass_low` and `mass_high` to -1.

321 • The minimal values for `ncall1`, `itmx1`, `ncall2`, `itmx2` are 250000,
322   5, 1000000, 5 for the DMV model, respectively. In order to increase
323   speed, set `foldsci` and `foldy` to 2 and keep `foldphi` at 1.

324 • The minimal values for `ncall1`, `itmx1`, `ncall2`, `itmx2` are 100000, 5,
325   100000, 5 for the DMS_tloop model, respectively.

326 • Allow negative weights for the DMV model by setting `withnegweights`
327   to 1.

328 • Since the DMS_tloop model is a leading order process, set `LOevents`
329   and `bornonly` are set to 1 internally.

1.4 *Colored scalar mediator, t-channel exchange*

331 An alternative set of simplified models exist where the mediator is
332 exchanged in the *t*-channel, thereby coupling the quark and dark
333 matter particle directly. Under the assumption that χ is a Standard
334 Model (SM) singlet, the mediating particle, labeled ϕ, is necessarily
335 charged and coloured. This model is parallel to, and partially mo-
336 tivated by, the squark of the MSSM, but in this case the χ is chosen
337 to be Dirac. Following the example of Ref. [PVZ14], the interaction
338 Lagrangian is written as

$$\mathcal{L}_{\text{int}} = g \sum_{i=1,2,3} (\phi_L^i \bar{Q}_L^i + \phi_{uR}^i \bar{u}_R^i + \phi_{dR}^i \bar{d}_R^i)\chi \qquad (1.23)$$

339 (Note: [PVZ14] uses only i = 1,2, but I think it's fine to extend this
340 to 3 here.) where Q_L^i, u_R^i and d_R^i are the SM quarks and ϕ_L^i, ϕ_{uR}^i and
341 ϕ_{dR}^i are the corresponding mediators, which (unlike the *s*-channel
342 mediators) must be heavier than χ. These mediators have SM gauge
343 representations under $(SU(3), SU(2))_Y$ of $(3,2)_{-1/6}$, $(3,1)_{2/3}$ and
344 $(3,1)_{-1/3}$ respectively. Variations of the model previously studied
345 include coupling to the left-handed quarks only [CEHL14, BDSJ⁺14],
346 to the ϕ_{uR}^i [DNRT13] or ϕ_{dR}^i [PVZ14, A⁺14], or some combina-
347 tion [BB13, AWZ14].

348   Minimal Flavour Violation (MFV) requires that the mediator
349 masses for each flavour be equal; the same logic also applies to the
350 couplings g. The available parameters are then

$$\{m_\chi, M_\phi, g\}. \qquad (1.24)$$

351   In practice, the third mediator mass and coupling could be sep-
352 arated from the other two, if higher order corrections to the MFV
353 prediction arise due to the large top Yukawa coupling – a common

variation is then to define this split between the first two generations and the third, so the parameters are extended to

$$\{m_\chi, M_{\phi_{1,2}}, M_{\phi_3}, g_{1,2}, g_3\}. \tag{1.25}$$

The width of each mediator is expressed, using the example of decay to an up quark, as

$$\Gamma(\phi_i \rightarrow \bar{u}_i \chi) = \frac{g_i^2}{16\pi M_{\phi_i}^3} (M_{\phi_i}^2 - m_{u_i}^2 - m_\chi^2)$$
$$\times \sqrt{M_{\phi_i}^4 + m_{u_i}^4 + m_\chi^4 - 2M_{\phi_i}^2 m_{u_i}^2 - 2M_{\phi_i}^2 m_\chi^2 - 2m_{u_i}^2 m_\chi^2},$$
$$\tag{1.26}$$

this reduces to

$$\frac{g_i^2 M_{\phi_i}}{16\pi} \left(1 - \frac{m_\chi^2}{M_{\phi_i}^2}\right)^2 \tag{1.27}$$

in the limit $M_{\phi_i}, m_\chi \gg m_{u_i}$.

An interesting point of difference with the s-channel simplified models is that the mediator can radiate a SM object, such as a jet or gauge boson, thus providing three separate mono-X diagrams which must be considered together in calculations. This model can also give a signal in the di-jet + MET channel when, for example, the χ is exchanged in the t-channel and the resulting ϕ pair each decay to a jet + χ.

2

Specific models for signatures with heavy flavor quarks

2.1 $b\bar{b}$+MET models

2.2 Models with a single $b-$quark + MET

2.3 $t\bar{t}$+MET models

As described in Section 1.2, one of the most simple UV complete extension of the effective field theory approach is the addition of a scalar mediator between DM and SM. A gauge singlet mediator can have tree-level interactions with a singlet DM particle that is either a Dirac or Majorana fermion, or DM that is a scalar itself. The spin-0 mediator can either be a real or complex scalar; a complex scalar contains both scalar and pseudoscalar particles, whereas the real field only contains the scalar particle. In this document we consider only two of the possible choices for this simplified model: one where the interaction with the SM is mediated by a real scalar, and the second where we consider only a light pseudoscalar, assuming that the associated scalar is decoupled from the low-energy spectrum. The kinematics of the two cases is sufficiently different to suggest that further investigation of the complex scalar case is needed but left for future studies.

Couplings to the SM fermions can be arranged by mixing with the SM Higgs. Such models have interesting connections with Higgs physics, and can be viewed as generalizations of the Higgs portal to DM. The most general scalar mediator models will have renormalizable interactions between the SM Higgs and the new scalar ϕ or pseudoscalar a, as well as ϕ/a interactions with electroweak gauge bosons. Such interactions are model dependent, often subject to constraints from electroweak precision tests, and would suggest specialized searches which cannot be generalized to a broad class of models (unlike, for instance, the $\not{E}_T +$ jets searches). As a result, for this class of minimal simplified models with spin-0 mediators, we will focus primarily on couplings to fermions and loop-induced couplings to

399 gluons. Possible couplings to the electroweak sector may also lead to
400 interesting DM phenomenology that can be studied in the context of
401 Higgs Portal DM.

402 *2.3.1   Model and assumption for fermionic DM*

403 Minimal Flavor Violation (MFV) implies that scalar couplings to
404 fermions will be proportional to the fermion mass. However, they can
405 differ for up- and down-type quarks and for charged leptons.
406   Following the assumption that DM is a fermion χ, which couples
407 to the SM only through a scalar ϕ or pseudoscalar a, the most general
408 tree-level Lagrangians compatible with the MFV assumption are [**? ?**
409]:

$$
\begin{aligned}
\mathcal{L}_{\text{fermion},\phi} \;=\;& \mathcal{L}_{\text{SM}} + i\bar{\chi}\slashed{\partial}\chi + m_\chi \bar{\chi}\chi + \left|\partial_\mu \phi\right|^2 + \frac{1}{2}m_\phi^2 \phi^2 + \\
& g_\chi \phi \bar{\chi}\chi + \frac{\phi}{\sqrt{2}} \sum_i \left(g_u y_i^u \bar{u}_i u_i + g_d y_i^d \bar{d}_i d_i + g_\ell y_i^\ell \bar{\ell}_i \ell_i \right) ,
\end{aligned}
\tag{2.1}
$$

$$
\begin{aligned}
\mathcal{L}_{\text{fermion},a} \;=\;& \mathcal{L}_{\text{SM}} + i\bar{\chi}\slashed{\partial}\chi + m_\chi \bar{\chi}\chi + \left|\partial_\mu a\right|^2 + \frac{1}{2}m_a^2 a^2 + \\
& i g_\chi a \bar{\chi}\gamma_5 \chi + \frac{ia}{\sqrt{2}} \sum_i \left(g_u y_i^u \bar{u}_i \gamma_5 u_i + g_d y_i^d \bar{d}_i \gamma_5 d_i + g_\ell y_i^\ell \bar{\ell}_i \gamma_5 \ell_i \right)
\end{aligned}
\tag{2.2}
$$

410 Here the sums run over the all SM generations; the Yukawa couplings
411 y_i^f are normalized to $y_i^f = \sqrt{2}m_i^f/v$ where $v \simeq 246\,\text{GeV}$ represents
412 the Higgs vacuum expectation value (VEV). We parametrise the DM-
413 mediator coupling as g_χ, without any additional Yukawa structure
414 between the mediator and the dark sector.
415   The most general Lagrangians including new scalars or pseu-
416 doscalars will have a potential containing interactions with the SM
417 Higgs field h. As already stated we only choose a minimal set of in-
418 teractions that do not include interactions with the Higgs field. Given
419 this simplification, the minimal set of parameters under consideration
420 is

$$
\left\{ m_\chi,\; m_{\phi/a},\; g_\chi,\; g_u,\; g_d,\; g_\ell \right\} .
\tag{2.3}
$$

421 The simplest choice of couplings, known as Minimal Simplified Dark
422 Matter model (MSDM) **[TODO: add references]**, is $g_u = g_d = g_\ell$,
423 which is realized in singlet scalar extensions of the SM.
424   Extending the SM Higgs sector to a two Higgs doublet model im-
425 plies more complex couplings such as $g_u = \cot\beta$ and $g_d = g_e = \tan\beta$
426 where $\tan\beta$ denotes the ratio of VEVs of the two Higgs doublets. The
427 case $g_u \neq g_d \neq g_\ell$ requires more additional scalars with potentially
428 large masses, and it is not covered here: for simplicity, we assume
429 universal SM-mediator couplings $g_v = g_u = g_d = g_\ell$ in the remainder
430 of this work.

431   The expected signal of DM pair production depends on the pro-
432 duction rate defined by the dark matter mass m_χ, mediator $m_{\phi/a}$, on
433 the couplings g_i and on the branching ration defined by the total de-
434 cay width of the mediator ϕ/a. We calculate the minimum possible
435 width (assuming only decays into the dark matter and the Standard
436 Model fermions) that is consistent with a given value of $g_\chi g_{SM}$. These
437 are given by Eq. (2.4) [BFG15].

$$
\Gamma_{\phi,a} = \sum_f N_c \frac{y_f^2 g_v^2 m_{\phi,a}}{16\pi} \left(1 - \frac{4m_f^2}{m_{\phi,a}^2}\right)^{3/2} + \frac{g_\chi^2 m_{\phi,a}}{8\pi} \left(1 - \frac{4m_\chi^2}{m_{\phi,a}^2}\right)^{3/2}
$$

$$
+ \frac{\alpha_s^2 y_t^2 g_v^2 m_{\phi,a}^3}{32\pi^3 v^2} \left| f_{\phi,a}\left(\frac{4m_t^2}{m_{\phi,a}^2}\right) \right|^2
\tag{2.4}
$$

438   where

$$
f_\phi(\tau) = \tau\left[1 + (1-\tau)\arctan^2\left(\frac{1}{\sqrt{\tau-1}}\right)\right], \qquad f_a(\tau) = \tau\arctan^2\left(\frac{1}{\sqrt{\tau-1}}\right). \tag{2.5}
$$

439   The first term in each width corresponds to the decay into SM
440 fermions, and the sum runs over all kinematically available fermions,
441 $N_c = 3$ for quarks and $N_c = 1$ for leptons. The second term is the
442 decay into DM, assuming that is kinematically allowed. The factor
443 of two between the decay into SM fermions and into DM is a result
444 of our choice of normalization of the Yukawa couplings due to spin
445 dependencies. The last two terms correspond to decay into gluons.
446 Since we have assumed that $g_v = g_u = g_d = g_\ell$, we have included in
447 the partial decay widths $\Gamma(\phi/a \to gg)$ only the contributions stem-
448 ming from top loops, which provide the by far largest corrections
449 given that $y_t \gg y_b$ etc. At the loop level the mediators can decay not
450 only to gluons but also to pairs of photons and other final states if
451 kinematical accessible. However the decay rates $\Gamma(\phi/a \to gg)$ are
452 always larger than the other loop-induced partial widths, and in con-
453 sequence the total decay widths $\Gamma_{\phi/a}$ are well approximated by the
454 corresponding sum of the individual partial decay widths involving
455 DM, fermion or gluon pairs. It should be noted that if $m_{\phi/a} > 2m_t$
456 the total widths of ϕ/a will typically be dominated by the partial
457 widths to top quarks.

458 2.3.2   *Parameter scan*

459 As discussed in Sec. **??**, the MFV assumption for spin-0 mediators
460 leads to quark mass dependent Yukawa couplings, and therefore
461 dominant couplings to top quarks. This motivates dedicated DM+$t\bar{t}$
462 searches. The benchmark chosen for these searches follows the as-
463 sumptions mentioned in the previous Section: we consider a Dirac

fermion DM particle, universal couplings to quarks, and minimum mediator width.

The benchmark points scanning the model parameters have been selected to ensure that the kinematic features of the parameter space are sufficiently represented. Detailed studies were performed to identify points in the m_χ, $m_{\phi,a}$, g_χ, g_v (and $\Gamma_{\phi,a}$) parameter space that differ significantly from each other in terms of expected detector acceptance. Because missing transverse momentum is the key observable for searches, the mediator p_T spectra is taken to represent the main kinematics of a model. Another consideration in determining the set of benchmarks is to focus on the phase space where we expect the searches to be sensitive during the 2015 LHC run. Based on a projected integrated luminosity of $30\,\mathrm{fb}^{-1}$ expected for 2015, we disregard model points with a cross section times branching ratio smaller than $0.1\,\mathrm{fb}$.

2.3.3   Parameter scan

The kinematics is most dependent on the masses m_χ and $m_{\phi,a}$. Figure 2.1 and 2.2 show typical depenencies for for scalar and pseudoscalar couplings respectively.

The two relevant thresholds that are observed for the variation in the kinematic spectra are $m_{\phi,a} = 2m_\chi$ and $m_{\phi,a} = 2m_t$. When the mediator mass exceeds both these thresholds then the p_T spectra broadens with larger $m_{\phi,a}$ and the kinematics for ϕ and a are comparable. The mediator p_T spectra changes significantly when crossing these thresholds. In particular, the kinematics are different for an on-shell mediator compared to an off-shell mediator ($m_{\phi,a} < 2m_\chi$). Furthermore, the scalar case differs from the pseudoscalar one when $m_\phi < 2m_t$. Therefore, it is important to have benchmark points covering both sides of these thresholds with sufficient granularity.

Typically only weak dependencies on width or equivalently couplings are observed (see Fig 2.4), except for large mediator masses of $\sim 1.5\,\mathrm{TeV}$ or for very small couplings of $\sim 10^{-2}$. These regimes where width effects are significant have production cross sections that are too small to be relevant for $30\,\mathrm{fb}^{-1}$ and are not considered here. However, with the full Run-2 dataset, such models may be within reach. The weak dependence on the typical width values can be understood as the parton distribution function are the dominant effect on mediator production. In other words, for couplings $\sim O(1)$ the width is large enough that the p_T of the mediator is determined mainly by the PDF.

Another case where the width can impact the kinematics is when $m_{\phi,a}$ is slightly larger than $2m_\chi$. Here, the width determines the rel-
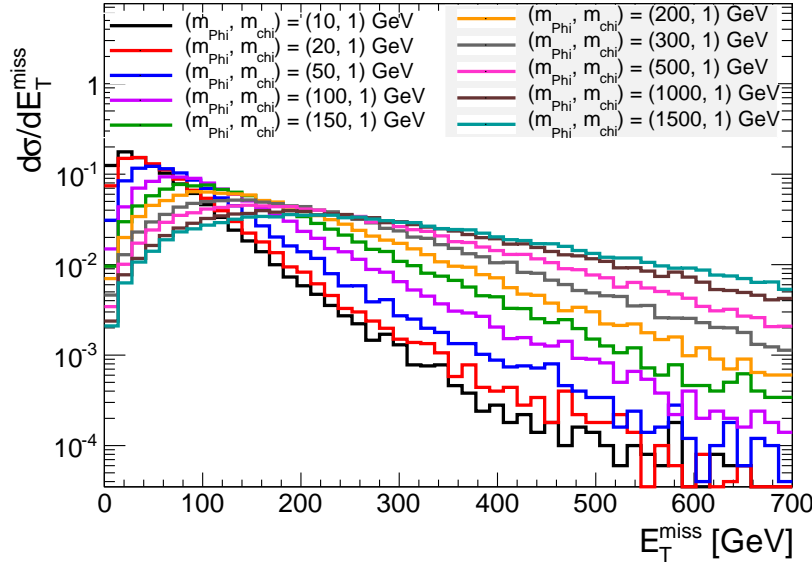
Figure 2.1: Example of the dependence of the kinematics on the scalar mediator mass. The Dark Matter mass is fixed to be 1GeV.
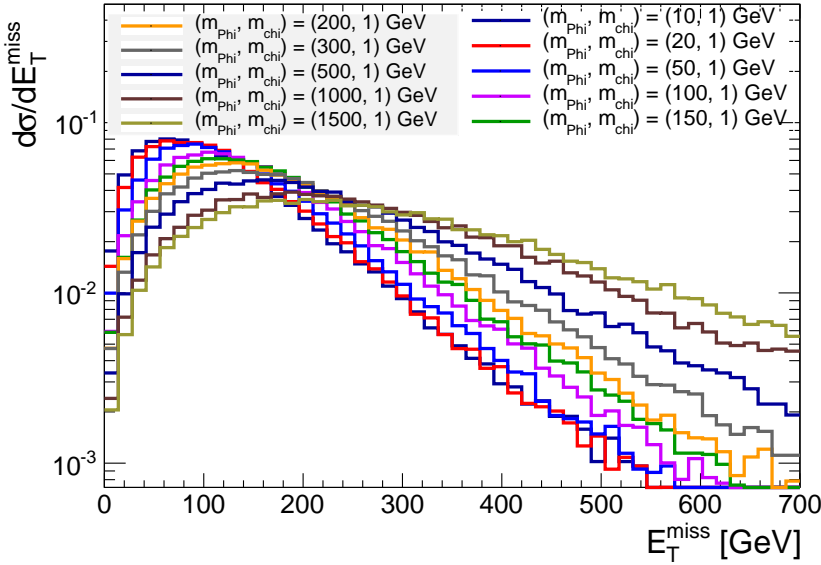

Figure 2.2: Example of the dependence of the kinematics on the pseudoscalar mediator mass. The Dark Matter mass is fixed to be 1GeV.

ative contribution between on-shell and off-shell production. An example is given in Fig. 2.5. In our recommendations we propose to use for semplicity the minimal width, as this is represents the most conservative choice to interpret the LHC results. **[TODO: mention**
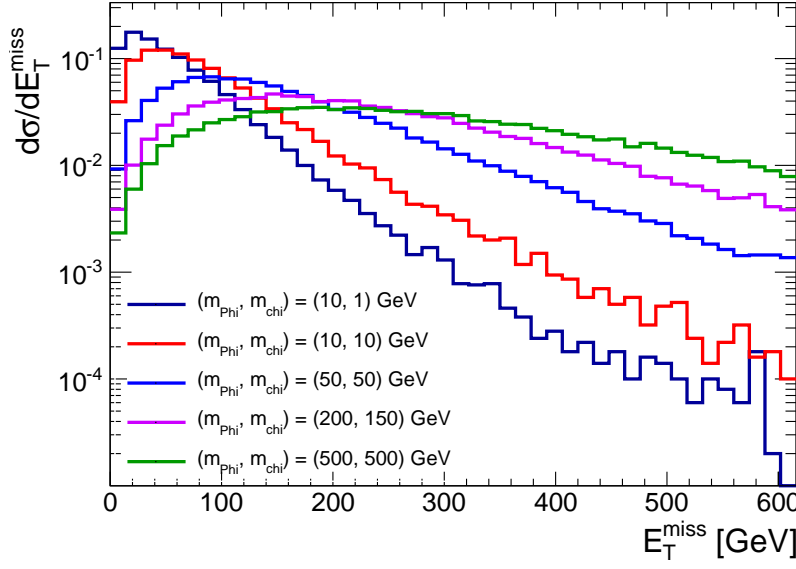
Figure 2.3: Example of the dependence of the kinematic for points of the grid proposed in Tab. **??** close to the $m_{\phi,a} \sim 2m_\chi$ limit.3

Figure 2.4: Study of the dependence of kinematics on the width of a scalar mediator. The width is increased up to four times the minimal width for each mediator and dark matter mass combination.

larger widths too]

Given that the kinematics are similar for all couplings $\sim O(1)$, we recommend to generate only samples with $g_\chi = g_v = 1$. It follows

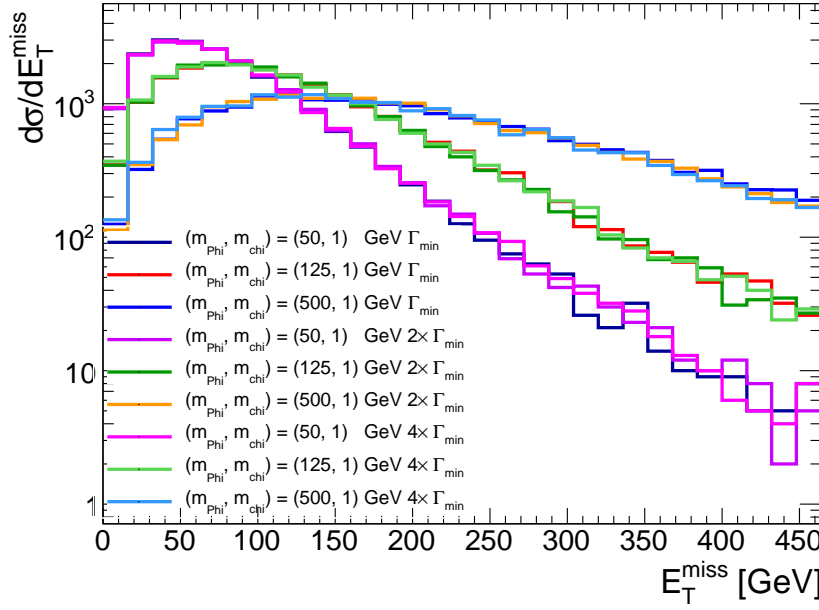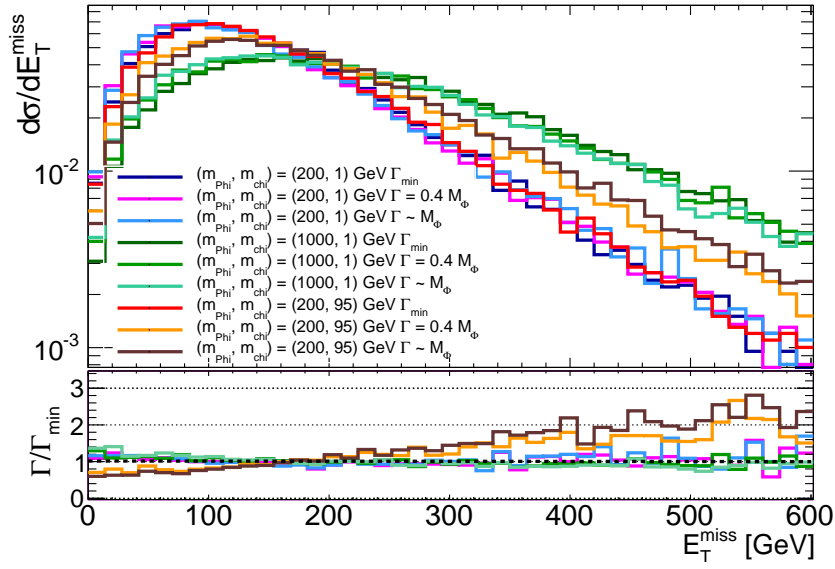Figure 2.5: Dependence of the dependence of kinematics on the width of a scalar mediator. The width is increased up to the mediator mass. Choices of mediator and dark matter masses such that $m_{\phi,a}$ is slightly larger than $2m_\chi$ is the only case that shows a sizeable variation of the kinematics as a function of the width.

from this that these benchmark points should be a good approximation for non-unity couplings and for $g_\chi \neq g_v$, provided that the sample is rescaled to the appropriate cross section times branching ratio. While a simple scaling function **[CD: which?]** is sufficient for a limited range of coupling values (see Fig. 2.6 for example), we also choose to provide instead a table of cross section times branching ratio values over a large range of couplings to support interpretation of search results (see the Appendix **??**). The table lists couplings from $g = 0.1$ to $g = 3.5$, where the upper limit is chosen to close to the perturbative limit.

The points for the parameter scan chosen for this model are listed in Table **??**, chosen to be harmonized with those for other analyses employing the same scalar model as benchmark. In addition to the considerations discussed in the preceding subsections, very light DM fermions are included ($m_\chi = 10\,\text{GeV}$) as this is a region where colliders have a complementary sensitivity to current direct detection experiments.

2.4 Models with a single top−quark + MET

[TODO: find a consistent notation for Xnew, M, V and Madgraph model]

A dark matter candidate χ and a new particle M (vector or scalar) are added to the SM, in an effective theory that respects the $SU(2)_L \times$
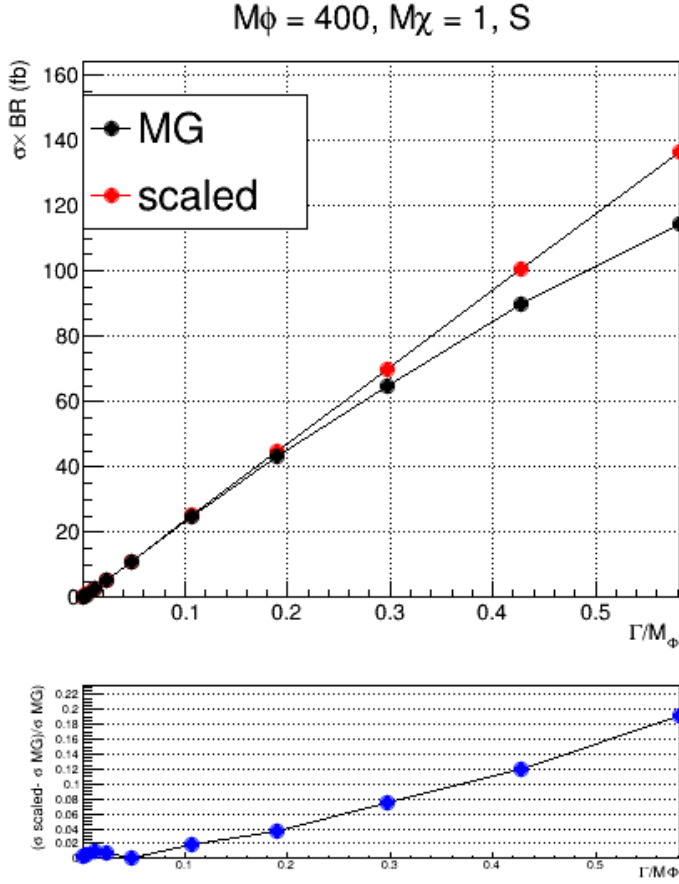
Figure 2.6: An example comparing a simple cross section scaling versus the computation from the generator, for a scalar model with $m_\phi = 400\,\mathrm{GeV}$ and $m_\chi = 1\,\mathrm{GeV}$. In this example, the scaling relationship holds for Γ_ϕ/m_ϕ below 0.2, beyond which finite width effects become important and the simple scaling breaks down.

$U(1)_Y$ symmetry and produces a single top quark in association with either the DM particle or the new particle (generally called X_{new} when no distinction is made). The full details of these models are described in [AFM11, AAB$^+$14, BCDF15].

There are two classes of models based on the monotop production mode: resonant and non-resonant production, as shown in Fig. 2.7.

The following two sections describe the phenomenology leading to these two production mechanisms. Depending on the nature of X_{new}, two main final states might be relevant: monotop production or same-sign top quark pair production. The interplay of these two signatures can largely probe this class of dark matter model, but a detailed study of their complementarity is beyond the scope of this Forum report.
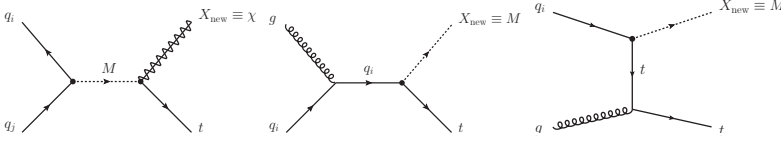
Figure 2.7: Feynman diagram of leading order processes leading to monotop events: resonant production of t via resonant new particle M decaying into a top quark and X_{new}, which is the dark matter fermion χ (left), and s and t channel non-resonant production of a top quark in association with X_{new}, which is the new particle M (middle and right).

RESONANT PRODUCTION

In this case, the new particle M is a coloured 2/3-charged scalar $\phi^\pm$ decaying into a top quark and a spin-1/2 invisible particle, χ (in this case X_{new} is the dark matter candidate χ). The dynamics of the new sector is then described by the following Lagrangian:

$$\mathcal{L} = d_i^C \left[(g_{\phi d}^v)^{ij} + (g_{\phi d}^a)^{ij} \gamma^5 \right] d_j\, \phi^\pm + u_k^C \left[(g_{u\chi}^v)^k + (g_{u\chi}^a)^k \gamma^5 \right] \chi\, \phi^\pm \quad (2.6)$$

where u (d) stands for any up-quark ($down$-quark), the index v (a) stands for vectorial (axial), C means charge conjugate and i, j, k run over the generations (color indices involved in the $\phi^\pm-$quarks interaction are not explicitly written). The first term leads to the production of the new particle and the last term allows its decay into a up-quark and a non interacting fermion (in particular to the top quark when $(g_{u\chi}^{v/a})^k$ is sizable mainly for $k = 3$). This model is then described by the masses of the new particle m_ϕ and the invisible fermion m_χ, and the coupling $(g_{\phi d}^{v/a})^{ij}$ and $(g_{u\chi}^{v/a})^k$.

NON-RESONANT PRODUCTION

For the non-resonant production, the top quark is produced in association with the new particle (X_{new} is then the new particle and not the dark matter candidate). The new particle can be either a new scalar, interacting with the SM and the DM candidate, or a new vector. For simplicity, we only consider the case of a vector new particle, as the scalar case would involve a mixing with the SM Higgs boson and therefore a larger parameter space.

The dynamics of a case with a vector new particle follows this Lagrangian:

$$\mathcal{L} = \bar{u}_i [(g_{Vu}^v)^{ij} \gamma^\mu + (g_{Vu}^a)^{ij} \gamma^5] u_j\, V_\mu + \bar{\chi} [g_{V\chi}^v \gamma^\mu + g_{V\chi}^a \gamma^5] \chi\, V_\mu \quad (2.7)$$

where u stands for any up-quark, the index v (a) stands for vectorial (axial) and i, j, k run over the generations. The first term describes the interaction between the new particle and the up-quarks while the second term leads to the decay the new particle into invisible fermions. The new sector can be defined with the couplings $(g_{Vu}^{v/a})^{ij}$, $g_{V\chi}^{a/v}$ and the masses m_V and m_χ. This model can be probed by two different experimental signatures: monotop and same-sign top quark production.

578 MODEL PARAMETERS AND ASSUMPTIONS

579   The models considered as benchmarks for the first LHC searches
580 contain further assumptions in terms of the flavour and chiral struc-
581 ture of the model with respect to the full Lagrangians from equa-
582 tions (2.6) and (2.7). These assumptions lead to limitations in LHC
583 constraints of the parameter space of these models, qualitatively dis-
584 cussed below.

585 *Assumptions in the flavour structure of the models*   In order to be visible
586 at the LHC in the monotop final state, these models must include a
587 strong coupling between the new particle ϕ and $t\chi$. In the resonant
588 case, the new particle must also couple to light quarks in order to
589 be produced at the LHC, leading to possible constraints from dijet
590 searches. The same kind of assumption exists for the non-resonant
591 production. The new particle M must be produced from a light
592 quark in the initial state, in association with a top quark: this sig-
593 nature can mainly probe a high coupling $\left(g_{Vu}^{v/a}\right)_{Vu}^{13} \equiv g_{Vtu}^{v/a}$. Therefore,
594 the sensitivity to other flavour couplings is significantly lower, since
595 V would be produced at a lower rate.

Assumptions in the chiral structure of the models   We only consider
right-handed quark components, in order to simplify the phenomenol-
ogy. The representation of the left-handed components under the
$SU(2)_L$ symmetry would a coupling to *down*-type quarks, since the
effective theory is invariant under $SU(2)_L \times U(1)_Y$ gauge symmetry.
Having a coupling between the new particle and *down*-type quarks
complicates the collider phenomenology in terms of decay modes.
Typically, including the left-handed components of quarks in the
lagrangian (2.7) describing the Vtu vertex would lead to

$$\mathcal{L}_{Vtu} = g_{Vtu}^{R}\, \bar{t}_R \gamma^\mu u_R\, V_\mu + g_{Vtu}^{L}(\bar{t}_L \gamma^\mu u_L + \bar{b}_L \gamma^\mu d_L)\, V_\mu \qquad (2.8)$$

596 where $g^{R/L} \equiv 1/2\,(g^v \pm g^a)$ couples only to right-handed/left-
597 handed components. The second term stems from invariance under
598 $SU(2)_L$ rotations, and leads to an additional decay mode $V \to b\bar{d} + \bar{b}d$
599 (on top of $V \to t\bar{u} + \bar{t}u$ and $V \to \chi\chi$). **[Open point: do we just set**
600 **the 2nd term to zero in this model? Justification?]**

601 IMPLEMENTATION AND NOTATION

602   This Section describes the notations used in the MadGraph model [Fuk]
603 convention, in term of the ones introduced in the previous Section.
604   The Madgraph model corresponds to the Lagrangian from [AFM11].
605 Each coupling constant of this dynamics can be set via the paramater
606 card and the blocks which are relevant for the two models used for
607 the experimental searches are described below.

608   1. Resonant scalar model described by the Lagrangian (2.6)

609   • AQS and BQS: 3×3 matrices (flavour space) fixing the coupling
610   of the scalar $\phi^{\pm}$ (S stands for scalar) and *down*-type quarks (Q
611   stands for quarks), written in this note $g_{\phi u}$ or a^q_{res}.

612   • A12S and B12S: 3×1 matrices (flavour space) fixing the coupling
613   of the fermion χ (12 stands for spin-1/2 fermion) and *up*-type
614   quarks, written in this note $g_{u\chi}$ or $a^{1/2}_{\text{res}}$.

615   • particle name: the scalar $\phi^{\pm}$ is labelled S and the fermion χ is
616   f_{met}

617   2. Non-resonant vectorial model described by the Lagrangian (2.7)

618   • A1FC and B1FC: 3×3 matrices (flavour space) fixing the coupling
619   of the vector V (1 stands for vector) and *up*-type quarks, written
620   in this note g_{Vu} or $a_{\text{non}-\text{res}}$.

621   • particle name: the vector V is labelled v_{met} and the fermion χ
622   doesn't exist

623   • the dark matter candidate χ is not implemented (this model
624   assumes $\text{BR}(V \rightarrow \chi\chi) = 100\%$)

625   A means vectorial coupling (g^v) and B means axial coupling (g^a) and
626   these two matrices are taken to be equal according to the chiral as-
627   sumptions made above. The convention adopted follows [ATL15] in
628   defining a single number a_{res} ($a_{\text{non}-\text{res}}$) for the resonant (non res-
629   onant) model, such as $(a^q_{\text{res}})_{12} = (a^q_{\text{res}})_{21} = (a^{1/2}_{\text{res}})_3 \equiv a_{\text{res}}$ (in
630   order to have $d - s - S$ couplings, and $t - S - f_{met}$ couplings) and
631   $(a_{\text{non}-\text{res}})_{13} = (a_{\text{non}-\text{res}})_{31} \equiv a_{\text{non}-\text{res}}$ (in order to have $v_{met} - t - u$
632   couplings).

633   PARAMETER SCAN
634   **[Open point - parameter scan studies go here.]**
635   Which parameters impact the kinematics (this is the only relevant
636   aspect form the experimental point of view)? Some studies would be
637   nice to put in this documents about:

638   • mediator mass

639   • mediator width: no effect (or parametrizable effects, plots are
640   ready and need to be included)

641   • **which parameters** impact our experimental sensitivity? Which
642   plane should be scanned?

643   What are the relevant numerical range to explore? First guess
644   would be to follow the mono-top analysis.

645 PARAMETER CHOICES AND CROSS SECTIONS

646 **[Open point: update with new numbers]**

647 ATLAS has considered two models, a resonant and a non-resonant

648 production, using only right-handed top quarks in the lepton+jets

649 final state. The signal samples were produced with MADGRAPH5

650 v1.5.11 interfaced with PYTHIA 8.175, using the MSTW2008LO Parton

651 Distribution Function (PDF) set (lhapdf ID: 21000). The mass of the

652 top quark was set at 172.5 GeV. Dynamic renormalisation and fac-

653 torisation scales were used. The *MET* particle mass was varied, and

654 in the case of the resonant model the resonance mass was fixed at

655 500 GeV:

656 • Resonant model, *MET* particle mass: [0,100] GeV in 20 GeV steps

657 • Non-resonant model, *MET* particle mass: [0,150] GeV in 25 GeV

658 steps, [200,300] GeV in 50 GeV and [400,1000] GeV in 100 GeV

659 steps

660 The couplings a_{res} and $a_{\mathrm{non-res}}$ are set at a fixed value of 0.2. In

661 addition, two samples are produced for the resonant model for

662 $m(f_{\mathrm{met}}) = 100$ GeV, with coupling strengths fixed at $a_{\mathrm{res}} = 0.5$

663 and $a_{\mathrm{res}} = 1.0$, in order to check the effect of the resonance width on

664 the signal event kinematics. The total width of the resonance varies

665 quadratically with the coupling strength, corresponding to a width

666 of 3.5 GeV, 21.6 GeV, and 86.5 GeV at $a_{\mathrm{res}} = 0.2$, $a_{\mathrm{res}} = 0.5$, and

667 $a_{\mathrm{res}} = 1.0$, respectively.

668 The number of free parameters is reduced by assuming $(a_{\mathrm{res}}^q)_{12} =$

669 $(a_{\mathrm{res}}^q)_{21} = (a_{\mathrm{res}}^{1/2})_3 \equiv a_{\mathrm{res}}$ for the resonant model and $(a_{\mathrm{non-res}})_{13} =$

670 $(a_{\mathrm{non-res}})_{31} \equiv a_{\mathrm{non-res}}$ for the non-resonant model, all other elements

671 of these coupling matrices being equal to 0. For each model, the cou-

672 pling parameter a_{res} or $a_{\mathrm{non-res}}$ and the masses of the exotic particles

673 are independent.

674 The cross-sections as well as the width of the resonance for the

675 resonance model are shown in Table 2.1. The cross-section is slowly

676 decreasing when $m(f_{met})$ increases, and the values do not differ by

677 larger than 10%, due to the similarity of the kinematics, in the chosen

678 mass range.

679 For the non-resonant case, the cross-sections are given in Table 2.2

680 and are calculated with $a_{\mathrm{non-res}} = 0.2$. The cross-section diverges

681 when $m(v_{met})$ tends to 0 GeV. However, when the mass is exactly

682 0 GeV the cross-section has a finite value, due to the specificity of the

683 propagator for this massless spin-1 boson.

684 **[Open point: systematic uncertainties]**

$m(f_{met})$ [GeV]	σ_{lep} [pb]	σ_{had} [pb]	$\Gamma(\Phi)$ [GeV]
0	1.107	2.214	3.492
20	1.102	2.205	3.491
40	1.089	2.180	3.487
60	1.068	2.137	3.481
80	1.039	2.078	3.472
100	1.001	2.003	3.461
100 ($a_{res} = 0.5$)	6.091	12.13	21.63
100 ($a_{res} = 1.0$)	21.77	43.72	86.52

Table 2.1: Theoretical predictions for the product of the production cross-section of the scalar resonance, the branching ratio of its decay into a top quark and the invisible particle, and of the branching ratio of the top quark decay into a semi-leptonic (σ_{lep}) or fully-hadronic (σ_{had}) final state, in the resonance model. Values are given for a resonance of mass 500 GeV and for an effective coupling $a_{res} = 0.2$ (except for two masses), as a function of the mass $m(f_{met})$ of the neutral fermion. The total widths $\Gamma(\Phi)$ of the resonance are also shown.

$m(v_{met})$ [GeV]	σ_{lep} [pb]	σ_{had} [pb]
0	96.03	192.4
25	359.0	717.9
50	113.4	226.9
75	59.86	119.5
100	37.45	74.82
125	25.35	50.68
150	18.00	35.96
200	9.662	19.28
250	5.506	11.02
300	3.328	6.656
400	1.372	2.738
500	0.6345	1.270
600	0.3192	0.6354
700	0.1698	0.3383
800	0.09417	0.1883
900	0.05472	0.1091
1000	0.03259	0.06479

Table 2.2: Theoretical predictions for the product of the production cross-section of the invisible vector v_{met} and of a top quark, and of the branching ratio of the top quark decay into a semi-leptonic (σ_{lep}) or fully-hadronic (σ_{had}) final state, in the non-resonance model. Values are given for an effective coupling $a_{non-res} = 0.2$, as a function of the mass $m(v_{met})$ of the invisible state.

Bibliography

[A⁺14] Jalal Abdallah et al. Simplified Models for Dark Matter and Missing Energy Searches at the LHC. *arXiv:1409.2893*, 2014.

[A⁺15] Georges Aad et al. Search for new phenomena in final states with an energetic jet and large missing transverse momentum in pp collisions at $\sqrt{s} = 8$ TeV with the ATLAS detector. 2015.

[AAB⁺14] Jean-Laurent Agram, Jeremy Andrea, Michael Buttignol, Eric Conte, and Benjamin Fuks. Monotop phenomenology at the Large Hadron Collider. *Phys.Rev.*, D89(1):014028, 2014.

[AFM11] J. Andrea, B. Fuks, and F. Maltoni. Monotops at the LHC. *Phys.Rev.*, D84:074025, 2011.

[ATL14] Sensitivity to WIMP Dark Matter in the Final States Containing Jets and Missing Transverse Momentum with the ATLAS Detector at 14 TeV LHC. Technical Report ATL-PHYS-PUB-2014-007, CERN, Geneva, Jun 2014.

[ATL15] Search for a single-top quark produced in association with missing energy in proton-proton collisions at $\sqrt{s} = 8$ TeV with the ATLAS detector. *Eur. Phys. J. C*, 75:79, 2015.

[AWZ14] Haipeng An, Lian-Tao Wang, and Hao Zhang. Dark matter with *t*-channel mediator: a simple step beyond contact interaction. *Phys. Rev. D*, 89:115014, 2014.

[BB13] Yang Bai and Joshua Berger. Fermion Portal Dark Matter. *JHEP*, 11:171, 2013.

[BCDF15] Idir Boucheneb, Giacomo Cacciapaglia, Aldo Deandrea, and Benjamin Fuks. Revisiting monotop production at the LHC. *JHEP*, 1501:017, 2015.

[BDSJ⁺14] Giorgio Busoni, Andrea De Simone, Thomas Jacques, Enrico Morgante, and Antonio Riotto. On the Validity of the Effective Field Theory for Dark Matter Searches at the LHC Part III: Analysis for the t-channel. *JCAP*, 1409:022, 2014.

[BFG15] Matthew R. Buckley, David Feld, and Dorival Goncalves. Scalar Simplified Models for Dark Matter. *Phys.Rev.*, D91(1):015017, 2015.

[CEHL14] Spencer Chang, Ralph Edezhath, Jeffrey Hutchinson, and Markus Luty. Effective WIMPs. *Phys. Rev. D*, 89:015011, 2014.

[DNRT13] Anthony DiFranzo, Keiko I. Nagao, Arvind Rajaraman, and Tim M. P. Tait. Simplified Models for Dark Matter Interacting With Quarks. *JHEP*, 1311, 2013.

[Fuk] Benjamin Fuks. Monotop Effective Theory: MadGraph model. `http://feynrules.irmp.ucl.ac.be/wiki/Monotops`.

[HKR13] Ulrich Haisch, Felix Kahlhoefer, and Emanuele Re. QCD effects in mono-jet searches for dark matter. *JHEP*, 1312:007, 2013.

[HR15] Ulrich Haisch and Emanuele Re. Simplified dark matter top-quark interactions at the LHC. 2015.

[PVZ14] Michele Papucci, Alessandro Vichi, and Kathryn M. Zurek. Monojet versus the rest of the world I: t-channel models. *JHEP*, 2014.